Atomistic Insight into Orthoborate–Based Ionic Liquids: Force Field Development and Evaluation

ARTICLE *in* THE JOURNAL OF PHYSICAL CHEMISTRY B · JULY 2014

Impact Factor: 3.3 · DOI: 10.1021/jp503029d · Source: PubMed

5 AUTHORS, INCLUDING:

Yonglei Wang
Stockholm University
18 PUBLICATIONS **63** CITATIONS
SEE PROFILE

Faiz Ullah Shah
Luleå University of Technology
15 PUBLICATIONS **169** CITATIONS
SEE PROFILE

Oleg N Antzutkin
The University of Warwick
142 PUBLICATIONS **4,630** CITATIONS
SEE PROFILE

THE JOURNAL OF PHYSICAL CHEMISTRY B

Article

pubs.acs.org/JPCB

Atomistic Insight into Orthoborate-Based Ionic Liquids: Force Field Development and Evaluation

Yong-Lei Wang,*[,†] Faiz Ullah Shah,[‡] Sergei Glavatskih,[§,∥] Oleg N. Antzutkin,[‡,⊥] and Aatto Laaksonen*[,†,#]

[†]Department of Materials and Environmental Chemistry, Arrhenius Laboratory, Stockholm University, S-106 91, Stockholm, Sweden

[‡]Chemistry of Interfaces, Luleå University of Technology, S-971 87, Luleå, Sweden

[§]System and Component Design, KTH Royal Institute of Technology, S-10 044, Stockholm, Sweden

[∥]Mechanical Construction and Production, Ghent University, B-9000 Ghent, Belgium

[⊥]Department of Physics, Warwick University, CV4 7AL, Coventry, United Kingdom

[#]Stellenbosch Institute of Advanced Studies (STIAS), Wallenberg Research Centre, Stellenbosch University, Marais Street, Stellenbosch 7600, South Africa

Supporting Information

ABSTRACT: We have developed an all-atomistic force field for a new class of halogen-free chelated orthoborate-phosphonium ionic liquids. The force field is based on an AMBER framework with determination of force field parameters for phosphorus and boron atoms, as well as refinement of several available parameters. The bond and angle force constants were adjusted to fit vibration frequency data derived from both experimental measurements and *ab initio* calculations. The force field parameters for several dihedral angles were obtained by fitting torsion energy profiles deduced from *ab initio* calculations. To validate the proposed force field parameters, atomistic simulations were performed for 12 ionic liquids consisting of tetraalkylphosphonium cations and chelated orthoborate anions. The predicted densities for neat ionic liquids and the $[P_{6,6,6,14}][BOB]$ sample, with a water content of approximately 2.3−2.5 wt %, are in excellent agreement with available experimental data. The potential energy components of 12 ionic liquids were discussed in detail. The radial distribution functions and spatial distribution functions were analyzed and visualized to probe the microscopic ionic structures of these ionic liquids. There are mainly four high-probability regions of chelated orthoborate anions distributed around tetraalkylphosphonium cations in the first solvation shell, and such probability distribution functions are strongly influenced by the size of anions.

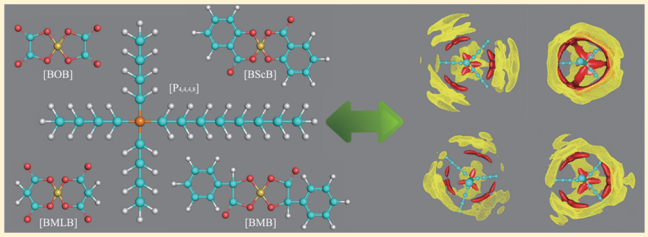

I. INTRODUCTION

Room-temperature ionic liquids (ILs) are special categories of molten salts usually composed of organic cations and, most commonly, inorganic anions,[1−3] that have melting points at or close to room temperature. Many ILs have attractive properties—such as negligible volatility, low flammability, and moderate viscosity—that make them good designer solvents for use toward the end goal of green chemistry. Hence, these ILs have attracted extensive attention in past decades due to their many potentially promising applications, such as in catalysis,[4−6] lubrication,[7] separation,[8] and electrochemistry.[9−11] Furthermore, through distinct combinations of cationic and anionic species, there is tremendous capacity to design solvents with tailored physical and chemical properties to meet specific requirements.

Tetraalkylphosphonium-based ILs are usually composed of four relatively large alkyl chains.[12−16] Such ILs are well-known for their thermal and chemical stabilities, which impart a practical advantage in industrial applications. The ILs composed of tetraalkylphosphonium cations and amino acid functionalized anions can be used as potential adsorbents for carbon dioxide capture, because they have a high affinity for CO_2 molecules, low glass transition temperatures, and high decomposition temperatures.[17−21] The ILs with tetraalkylphosphonium cations and a bis(trifluoromethylsulfonyl)imide anion exhibit quite wide electrochemical potential windows and relatively low degrees of ionicity due to strong ion pairing structures. The range of physicochemical properties of ILs can be extended by modifying the chemical architectures of corresponding ionic groups.[22,23]

Halogen-free chelated orthoborate ILs are a new type of task-specific ILs, consisting of tetraalkylphosphonium, pyrrolidinium, and imidazolium cations and stable chelated orthoborate anions, which can effectively escape hydrolysis in a range of applications.[24−27] As neat lubricants, the halogen-free orthoborate-phosphonium ILs exhibit lower friction and wear rates compared to fully formulated engine oil in steel−aluminum contacts.[26] The hydrolytic stabilities, low melting points, and

Received: March 27, 2014
Revised: June 7, 2014
Published: July 3, 2014

outstanding tribological properties for steel−aluminum contacts make these ILs attractive as alternative high-performance lubricants.

To tailor the physicochemical properties of currently available chelated orthoborate-phosphonium ILs and design other types of task-specific ILs with highly versatile physical and chemical properties, it is critical to understand the inherent relationship between the ILs' microscopic ionic structures and macroscopic properties.

Molecular simulations have proven indispensable for understanding the thermodynamic properties and ion pair structures of ILs at the molecular level.[28−33] First-principles quantum mechanics (QM) calculations provide a valuable technique to obtain useful information as a complement to experiments.[33] They are, however, very computation-intensive and can only be applied to systems of limited size. On the basis of molecular topologies, some properties, such as melting points[34] and viscosities,[35] can be predicted by empirical quantitative structure−property relationship methods.[34−36] However, these methods cannot accurately reveal the intrinsic relationship between microstructures and their macroscopic properties.

Atomistic classical molecular dynamics (MD) simulations are one of the most reliable and promising approaches for investigating structural and dynamic properties of molecular model systems.[30,37−42] By performing atomistic simulations, many research groups have reported the physical properties of 1-alkyl-3-methylimidazolium ILs over large temperature and pressure ranges.[37−39,43−50] Thermodynamic properties of pure ILs, including liquid densities and isothermal compressibility coefficients,[38,45−50] cohesive energy densities,[38,39] heats of vaporization,[37,39,48,49] microscopic structures,[37,44−46,48,50,51] and self-diffusion coefficients,[30,43−46,48,50] were systematically compared with available experimental data. In addition, simulation efforts were extended to the solvation structures and dynamics of small apolar particles[52] and inorganic ionic groups[53] in ILs.

The success of molecular simulations for accurately predicting various properties of a model system depends on the force field (FF) used, which refers to the functional forms and parameters used to describe the potential energy of the model system. Several FFs, including AMBER,[17,37,39,42,43,54] CHARMM,[38,40] OPLS,[41,46,49,55,56] and GROMOS[45] FFs, have been developed and successfully applied to a variety of IL systems. However, FFs developed for more specific categories of ILs have not yet been reported.

The aim of this work is to systematically construct a refined, all-atomistic FF for halogen-free chelated orthoborate-phosphonium ILs. The tetraalkylphosphonium cations studied in this work include tributyloctylphosphonium ([$P_{4,4,4,8}$]), tributyltetradecylphosphonium ([$P_{4,4,4,14}$]), and trihexyltetradecylphosphonium ([$P_{6,6,6,14}$]). The chelated orthoborate anions of interest are bis(mandelato)borate ([BMB]), bis(malonato)borate ([BMLB]), bis(oxalato)borate ([BOB]), and bis(salicylato)borate ([BScB]). Typical schematic structures of the [$P_{4,4,4,8}$] cation and these four chelated orthoborate anions are shown in Figure 1.

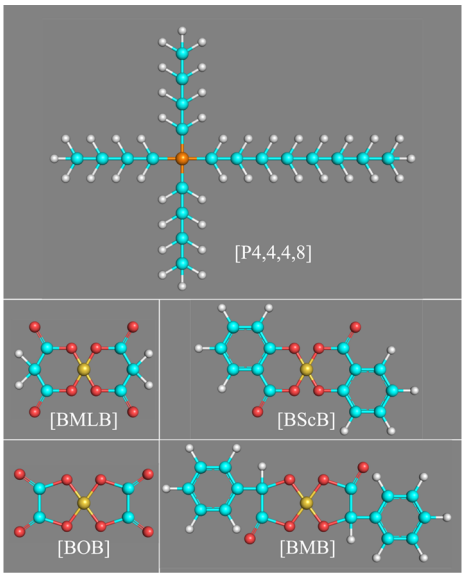

Figure 1. Schematic structures of tributyloctylphosphonium cation, [$P_{4,4,4,8}$], and four chelated orthoborate anions, including bis(malonato)borate, [BMLB]; bis(salicylato)borate, [BScB]; bis(oxalato)borate, [BOB]; and bis(mandelato)borate, [BMB].

II. FORCE FIELD DEVELOPMENT

Form of Potential Energy. The AMBER FF employs the following functional forms for potential energy U:

$$U_{\text{total}} = \sum_{\text{bonds}} K_r(r - r_0)^2 + \sum_{\text{angles}} K_\theta(\theta - \theta_0)^2 + \sum_{\text{torsions}} \frac{K_\phi}{2}[1 + \cos(n\phi - \gamma)] + \sum_{i<j} \left\{ 4\varepsilon_{ij}\left[\left(\frac{\sigma_{ij}}{r_{ij}}\right)^{12} - \left(\frac{\sigma_{ij}}{r_{ij}}\right)^{6}\right] + \frac{q_i q_j}{4\pi\varepsilon_0\varepsilon_r r_{ij}} \right\} \quad (1)$$

The first three terms represent the bonded interactions, i.e., bonds, angles, and torsions, and corresponding potential parameters have their usual meaning. The nonbonded interactions are described in the last term, including van der Waals (VdW, here the Lennard-Jones 12-6 form) and Coulombic interactions of atom-centered point charges. The VdW interactions are calculated between atoms in different molecules or atoms in the same molecule that are separated by more than three consecutive bonds. The VdW interaction parameters between different atoms are obtained from the Lorentz−Berthelot combining rule with $\varepsilon_{ij} = (\varepsilon_{ii}\varepsilon_{jj})^{1/2}$ and $\sigma_{ij} = (\sigma_{ii} + \sigma_{jj})/2$. The nonbonded interactions separated by exactly three consecutive bonds (1−4 interactions) are reduced by related scaling factors,[39,57] which are optimized as 0.50 for VdW interactions and 0.83 for electrostatic interactions, respectively.

Atom Types and van der Waals Parameters. In developing the FF parameters, the choice of suitable atom types is crucial. For tetraalkylphosphonium cations, the assignments of atom types are rather straightforward, since all atom types are well-defined in the AMBER FF. For chelated orthoborate anions, the atom type and corresponding VdW parameters of the boron (B) atom are missing in the AMBER FF, all of which are taken from the DREIDING FF.[58] The definition of atom types and VdW parameters of the other atoms in chelated orthoborate anions are assigned by using default AMBER FF parameters. The atom notations for the three tetraalkylphosphonium cations and four chelated orthoborate anions studied in this work are presented in

Figures S1 and S2 in the Supporting Information. The corresponding VdW parameters for all atom types are listed in Table 1.

Table 1. Nonbonded VdW Potential Parameters for Tetraalkylphosphonium Cations and Chelated Orthoborate Anions[a]

atom type	σ_{ii} (Å)	ε_{ii} (kJ/mol)	source
P	3.7422	0.8368	AMBER
CT	3.4001	0.4580	AMBER
HC	2.6498	0.0657	AMBER
HP	1.9602	0.0657	AMBER
B	3.5810	0.3974	DREIDING
C	3.4001	0.3601	AMBER
CA	3.4001	0.3601	AMBER
HA	2.5999	0.0628	AMBER
O	2.9603	0.8793	AMBER
O2	2.9603	0.8793	AMBER
OH	3.0668	0.8809	AMBER

[a]The notations of all atoms are shown in Figures S1 and S2 in the Supporting Information.

Optimized Geometries of Isolated Ions. The QM *ab initio* calculations were performed to optimize the isolated ionic structures using the Gaussian 09 package[59] at the B3LYP/6-311++G(d) level. Additional vibration analyses were then performed on optimized ionic geometries to ensure the absence of negative frequencies, and hence to verify the existence of a true minimum. Typical optimized geometries of the $[P_{4,4,4,8}]$ cation and four chelated orthoborate anions are shown in Figure S3 in the Supporting Information.

In the minimum conformers of tetraalkylphosphonium cations, each alkyl chain adopts an all-transoid conformation, and four alkyl chains take on typical tetrahedral arrangements around the central phosphorus (P) atom. This conformation is consistent with X-ray scattering data[60] and other QM *ab initio* results.[41,42,54]

For chelated orthoborate anions, the optimized ionic geometries are strongly influenced by corresponding chemical compositions. The most notable feature of the optimized ionic geometry of the [BOB] anion is that it displays two five-membered planar ring segments joined by the central B atom. The two planar segments are essentially perpendicular to each other, and the average O−B−O angle is approximately 109°, which is quite close to 108°, the experimental value verified by single-crystal X-ray diffraction.[27] For the [BMLB] anion, the addition of one carbon atom in each planar segment results in an unstable six-membered ring structure, which takes on a twisted conformation very similar to the boat conformation of a cyclic six-membered monosaccharide molecule.

Noteworthy, in [BMB] and [BScB] anions, the addition of two phenyl rings to central segments leads to different conformations compared to [BOB] and [BMLB] anions. The two five-membered rings in the central segments of the [BMB] anion take on similar planar conformations and are perpendicular to each other—which is similar to the conformation of the [BOB] anion—but two additional phenyl rings remain outside and have tilted conformations. Although the central segments in the [BScB] anion are similar to those in the [BMLB] anion and consist of two six-membered ring structures, the phenyl rings can form conjugated structures, which can eventually minimize the total conformational energy of the [BScB] anion. It should be noted that mandelic acid used in the synthesis of [BMB] anions is a chiral molecule. Therefore, [BMB] anions can be of three different types, namely, RR, SS, and RS, depending on whether R- or S-enantiomers (or both) of the mandelato group are considered. The effect of anion chirality on the physicochemical properties of imidazolium orthoborate ionic liquids was recently studied by Yu et al.[24] and Chiappe et al.[25] Only minor differences (<0.3°) in the temperature of solid−liquid transformation were found, while substantial variations in the thermal degradation temperature (ca. 10°) and in the optical rotation angle (ca. ±140°) were detected for ILs with the same cation but different enantiomers of [BMB] anions.[24] In the present work, the [BMB] anion adopted in subsequent *ab initio* calculations and atomistic simulations is of the RS type. Its optimized geometry is shown in Figure S3 in the Supporting Information.

Some structural parameters, such as bond lengths and covalent angles deduced from the optimized ionic geometries of the three tetraalkylphosphonium cations and four chelated orthoborate anions studied, are compared to available experimental X-ray scattering data[27,60−62] and listed in Tables S1−S3 in the Supporting Information. It is clearly shown that the optimized ionic geometries of tetraalkylphosphonium cations and chelated orthoborate anions, obtained from QM *ab initio* calculations, agree quite well with the available X-ray crystallographic data.[27,60−62] All the values of bond lengths and covalent angles in our proposed FF are listed in Tables 2 and 3.

Atomic Partial Charges. The method to determine atomic partial charges used in AMBER, known as the restraint electrostatic potential (RESP) fitting approach,[63] has been proven to be very efficient and successful for a variety of systems.[39,57,64] In this work, the one-conformation two-stage standard RESP method is used to derive atomic partial charges by fitting the molecular electrostatic potential generated from QM *ab initio* calculations at the B3LYP/6-311++G(d) level.

Table 2. Bond Stretching Potential Parameters for Tetraalkylphosphonium Cations and Chelated Orthoborate Anions[a]

bonds	r_0 (Å)	K_r (kJ/mol Å^2)	source	bonds	r_0 (Å)	K_r (kJ/mol Å^2)	source
P−CT	1.820	886.6	this work	CT−HC	1.090	1423.6	AMBER
CT−CT	1.526	1298.0	AMBER	CT−HP	1.090	1423.6	AMBER
B−O2	1.475	2927.4	this work	B−OH	1.450	2927.4	this work
C−C	1.409	1961.4	AMBER	C−O	1.219	2386.6	AMBER
C−O2	1.250	2746.7	AMBER	C−CT	1.522	1327.3	AMBER
CA−CT	1.510	1327.3	AMBER	CA−CA	1.400	1963.7	AMBER
CA−HA	1.080	1536.6	AMBER	CA−OH	1.332	1881.9	AMBER
CT−OH	1.410	1339.8	AMBER				

[a]The notations of all atoms are shown in Figures S1 and S2 in the Supporting Information.

Table 3. Angle Bending Potential Parameters for Tetraalkylphosphonium Cations and Chelated Orthoborate Anions[a]

angles	θ_0 (deg)	K_θ (kJ/mol rad^2)	source	angles	θ_0 (deg)	K_θ (kJ/mol rad^2)	source
P−CT−HP	106.7	171.5	this work	P−CT−CT	115.7	225.8	this work
CT−CT−CT	109.5	167.5	AMBER	CT−CT−HC	109.5	188.2	AMBER
CT−CT−HP	109.5	167.5	this work	CT−P−CT	109.5	209.1	this work
HP−CT−HP	106.5	146.5	this work	HC−CT−HC	109.5	146.5	AMBER
B−O2−C	115.5	418.2	this work	B−OH−CT	115.5	418.2	this work
B−OH−CA	115.5	418.2	this work	C−C−O	126.2	355.5	this work
C−C−O2	126.0	292.2	this work	C−CA−CA	120.0	263.8	AMBER
CA−CA−CA	120.0	263.8	AMBER	C−CT−C	114.6	263.5	this work
C−CT−CA	112.6	263.5	this work	C−CT−HC	109.5	209.1	AMBER
C−CT−OH	112.6	209.1	this work	CA−C−O	122.4	334.6	this work
CA−C−O2	117.0	292.8	this work	CA−CA−HA	120.0	146.5	AMBER
CA−CA−OH	120.0	292.8	AMBER	CA−CT−OH	112.6	209.1	AMBER
CA−CT−HC	109.5	209.1	AMBER	CT−C−O	120.4	335.0	AMBER
CT−C−O2	120.0	293.1	AMBER	CT−CA−CA	120.0	293.1	AMBER
HC−CT−OH	109.5	209.3	this work	O2−B−O2	109.5	418.2	this work
O2−B−OH	109.5	418.2	this work	OH−B−OH	109.5	418.2	this work
O2−C−O	126.6	335.0	this work				

[a]The notations of all atoms are shown in Figures S1 and S2 in the Supporting Information.

The computed atomic partial charges on each atom of three tetraalkylphosphonium cations and four chelated orthoborate anions are presented in Figures S1 and S2 in the Supporting Information.

Concerning the dipole moments of tetraalkylphosphonium cations and chelated orthoborate anions, to the best of our knowledge, there is no experimental data available in the literature. Thus, we compare the dipole moments deduced from the atomic partial charges obtained by RESP methodology with those derived from QM calculations by taking the atomic coordinates of P and B atoms as the origin of corresponding ionic groups. These comparisons, as illustrated in Table 4, indicate that the dipole moments obtained from QM *ab initio* calculations are well reproduced by RESP charges.

Table 4. Dipole Moments (in D) Obtained from QM *ab initio* Calculations (μ_{QM}) and from the Set of Atom-Centered Point Charges Deduced by the RESP Method (μ_{RESP})

ions	μ_{QM}	μ_{RESP}
[$P_{4,4,4,8}$]	6.7735	6.7808
[$P_{4,4,4,14}$]	20.2683	20.2360
[$P_{6,6,6,6}$]	0.0018	0.0012
[$P_{6,6,6,14}$]	14.8678	14.8760
[BMB]	4.9997	5.0071
[BMLB]	2.1601	2.1501
[BOB]	0.0005	0.0006
[BScB]	5.7848	5.8093

For tetraalkylphosphonium cations, we can observe that the difference in alkyl chain lengths is directly related to the dipole moments. The molecular geometry of tetraalkylphosphonium cations resembles T_d symmetry; hence, the total dipole moment of a tetraalkylphosphonium cation with four linear alkyl chains characterized by equal numbers of carbon atoms, such as [$P_{6,6,6,6}$] cation, is almost equal to zero. A larger difference in alkyl chain lengths results in a shift in the charge distribution center toward the longer alkyl substitute, and hence leads to a larger dipole moment.

For chelated orthoborate anions, [BOB] possesses a negligibly small dipole moment due to its symmetric composition where two perpendicular planar segments are joined by the central B atom. In the other three anions, the twisted molecular conformations and localized charge distributions in the phenyl substitutes contribute to large dipole moments.

For the symmetric [$P_{6,6,6,6}$] cation and [BOB] anion, the quadrupole and octupole moments obtained from RESP charges are consistent with those deduced from QM *ab initio* calculations, as illustrated in Table S4 in the Supporting Information.

Bond and Angle Force Constants. In general, once the optimized molecular geometries are obtained from QM *ab initio* calculations, the bond and angle force constants can be adjusted by fitting vibration frequencies to the corresponding model system. Due to limited vibration frequency data for tetraalkylphosphonium cations and chelated orthoborate anions, we performed QM *ab initio* calculations with vibration frequency analysis based on optimized molecular geometries to provide a valuable benchmark. The B3LYP method overestimates vibration frequencies by approximately 4%; therefore, a scaling factor of 0.9614 was adopted for B3LYP calculations.[65]

In this work, as suggested in previous literature,[37,39] molecular mechanics (MM) calculations were also performed utilizing a TINKER package.[66] The MINIMIZE and VIBRATE modules were employed to perform normal-mode analysis. Thus, vibration frequencies of a model system and corresponding vibration normal modes were obtained. These vibration frequencies were then used to fit the benchmark QM vibration results to determine bond and angle force constants for tetraalkylphosphonium cations and chelated orthoborate anions.

For tetraalkylphosphonium cations, the typical P−C stretching frequency obtained from QM *ab initio* calculations is 734.5 cm^{-1}, and the corresponding frequency fitted by MM calculations is 752.4 cm^{-1}. Both of these values are generally in satisfactory agreement with the experimental vibration frequency of 721 cm^{-1} obtained by Murphy et al.[67] and 737 cm^{-1} obtained in this work for [$P_{6,6,6,14}$][BMB] (see Table S5 in the Supporting Information). A detailed comparison of the vibration frequencies of the [$P_{6,6,6,14}$] cation obtained through

QM calculations, MM fittings, and experimental measurements is provided in Table S5 in the Supporting Information.

However, in the case of chelated orthoborate anions, several bond and angle force constants are missing in the AMBER FF, and it is very difficult to determine a global optimized set of force constants to fit all vibration frequencies because the assignments of frequency data have to be done manually. Hence, in this work, we mainly focus on the frequency of B−O2/OH stretching, which is the primary characteristic of vibration moments of chelated orthoborate anions. The typical B−O2/OH stretching frequencies obtained from QM calculations and MM fittings, as well as available experimental measurements, are shown in Table 5. Detailed comparisons of vibration frequencies of [BMB] and [BScB] anions from QM and MM calculations and available experimental data are shown in Tables S6 and S7 in the Supporting Information. The frequencies fitted from MM calculations are consistent with the ones obtained from QM calculations with a maximum deviation of 33 cm^{-1}, as well as with available experimental data with a maximum deviation of 44 cm^{-1}.

Table 5. Typical Stretching Frequencies (in cm^{-1}) for B−O2/OH Bonds in Chelated Orthoborate Anions Obtained from QM *ab initio* Calculations and Fitted from MM Calculations, as Well as Experimental FT-IR Measurements (See the Supporting Information)

	QM	MM	experimental data
[BMB]	1311.40	1321.41	1305.53
[BMLB]	1326.94	1342.71	
[BOB]	1324.84	1325.67	
[BScB]	1320.86	1317.14	1314.93

The final sets of bond and angle force constant parameters are listed in Tables 2 and 3.

Torsion Energy Barriers. For tetraalkylphosphonium cations and chelated orthoborate anions, there is no definition for several torsion angles in the current AMBER FF. The most important ones are those related to P and B atoms in the center of tetraalkylphosphonium cations and chelated orthoborate anions, respectively, which can strongly influence the rotation of lateral alkyl chains in cations and the stability of ring structures in anions.

In this work, QM *ab initio* torsion energy profiles were obtained using the Gaussian 09 package at the HF/6-311++G(d)//B3LYP/6-311++G(d) level. In geometry optimizations, all degrees of freedom were allowed, except the torsion angle of interest, which varies in a step of 10°. Furthermore, the optimized conformers from QM calculations were used directly for MM energy calculations by the ANALYZE module in the TINKER package.[66] Finally, the coefficients of the torsion angles were optimized to fit the QM torsion energy profiles for tetraalkylphosphonium cations and chelated orthoborate anions. The optimized torsion parameters in this work are listed in Table 6.

In Figure 2, we present the energy profiles for P−CT−CT−CT, P−CT−CT−HC, CT−P−CT−CT, and CT−P−CT−HP torsions of the $[P_{4,4,4,8}]$ cation obtained from QM and MM calculations. (For notations of all atoms, see Figures S1 and S2 in the Supporting Information.) Three torsion angles (P−CT−CT−HC, CT−P−CT−CT, and CT−P−CT−HP) exhibit a

Table 6. Dihedral Potential Parameters for Tetraalkylphosphonium Cations and Chelated Orthoborate Anions[a]

torsions	γ (deg)	K_ϕ (kJ/mol)	n	source	torsions	γ (deg)	K_ϕ (kJ/mol)	n	source
CT−CT−CT−CT	0.0	2.100	3	AMBER	CT−CT−CT−HC	0.0	1.340	3	AMBER
P−CT−CT−CT	0.0	1.340	3	this work	CT−P−CT−CT	0.0	18.820	1	this work
P−CT−CT−HC	0.0	1.260	3	this work	CT−P−CT−CT	0.0	1.340	3	this work
CT−CT−CT−HP	0.0	1.300	3	this work	CT−P−CT−HP	0.0	2.100	3	this work
HC−CT−CT−HC	0.0	1.260	3	AMBER	HC−CT−CT−HP	0.0	1.300	3	this work
B−O2−C−C	180.0	83.000	2	this work	O2−B−O2−C (i-r)	180.0	9.000	2	this work
B−O2−C−CA	180.0	8.364	2	this work	O2−B−O2−C (o-r)	0.0	4.200	3	this work
B−O2−C−CT	180.0	16.780	2	this work	O2−B−OH−CA (i-r)	180.0	8.400	2	this work
B−O2−C−O	180.0	30.780	2	this work	O2−B−OH−CA (o-r)	0.0	4.200	3	this work
B−OH−CA−CA	180.0	30.400	2	this work	OH−B−OH−CT	0.0	4.200	3	this work
B−OH−CT−C	180.0	8.400	2	this work	OH−B−O2−C (i-r)	180.0	8.400	2	this work
B−OH−CT−CA	180.0	8.400	2	this work	OH−B−O2−C (o-r)	0.0	4.200	3	this work
B−OH−CT−HC	0.0	8.400	3	this work	OH−B−OH−CA	0.0	4.200	3	this work
C−CT−C−O	0.0	12.560	2	this work	C−CT−C−O2	0.0	12.560	2	this work
CA−CA−C−O	180.0	30.400	2	this work	CA−CA−C−OH	0.0	1.308	3	this work
CA−CA−C−O2	180.0	30.400	2	this work	CA−CA−CA−OH	180.0	1.308	2	this work
HC−CT−C−O	0.0	6.720	1	AMBER	HC−CT−C−O	180.0	1.360	3	AMBER
O−C−CT−C	0.0	12.560	2	AMBER	O−C−CT−HC	180.0	1.360	3	AMBER
O−C−CT−OH	0.0	6.700	1	AMBER	O−C−CT−OH	180.0	0.690	3	AMBER
O−C−C−O2	0.0	63.000	2	this work	O−C−C−O	180.0	63.000	2	this work
O2−C−C−O2	180.0	83.000	2	this work	X−CA−CA−X	180.0	30.400	2	AMBER
					Improper Torsions				
CT−CA−CA−CA	180.0	9.248	2	AMBER	CT−CA−CA−HA	180.0	9.248	2	AMBER
C−CA−CA−CA	180.0	9.248	2	AMBER	OH−CA−CA−CA	180.0	9.248	2	AMBER
O2−C−O−C	180.0	16.800	2	this work	O2−CA−O−C	180.0	16.800	2	this work
O2−CT−O−C	180.0	16.800	2	this work					

[a]The i-r and o-r represent in-ring and out-of-ring torsions in chelated orthoborate anions, respectively. The notations of all atoms are shown in Figures S1 and S2 in the Supporting Information.

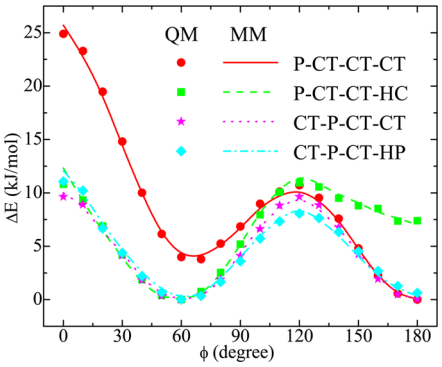

Figure 2. Torsion profiles of the dihedrals in tetraalkylphosphonium cations, obtained from QM (dots) and MM (lines) calculations in this work. The notations of all atoms are shown in Figures S1 and S2 in the Supporting Information.

simple energy profile with a 120° period and an energy barrier around 10 kJ/mol, both of which reflect the sp^3 character of the central atoms and the constrained nature of alkyl chains attached to the central P atom. The energy profile of P−CT−CT−CT, in which the energy barrier is approximately 25 kJ/mol, clearly reflects the more articulated feature of the all-transoid conformations of the alkyl chains.

For chelated orthoborate anions, [BMB] and [BOB] anions have similar five-membered ring structures, and [BMLB] and [BScB] anions have six-membered ring structures in central segments, respectively. Hence, corresponding related QM torsion energy profiles are only calculated for [BOB] and [BMLB] anions. Eight typical torsion energy profiles for [BOB] and [BMLB] anions obtained from QM and MM calculations are shown in Figure 3. The general feature of these torsion energy profiles is that all energy barriers are much higher due to the existence of ring structures. For most torsions, the equilibrium angles are around 0° (B−O2−C−C in [BOB]) and 180° (B−O2−C−O in [BOB]), which contribute to stable ring structures in corresponding anions. It should be noted that two O2−B−O2−C torsions in the [BOB] anion exhibit totally different energy profiles. The equilibrium torsion angle for the one inside five-membered ring is at 0° due to the planar ring structure, while, for the one between adjacent five-membered rings, the equilibrium dihedral angle is around 120°, which contributes to the perpendicular distributions of the two planar ring segments. The distinction between these two O2−B−O2−C torsions is shown in Table 6.

The QM and MM results presented above for isolated ions indicate that the proposed FF parameters can successfully mimic ionic structures and charge distributions. Although there are some minor deviations in predicting vibration frequencies, the proposed FF are then applied to liquid-state atomistic simulations on halogen-free chelated orthoborate-phosphonium ILs in the following section.

III. LIQUID-STATE ATOMISTIC SIMULATIONS

Simulation Details. The liquid-state atomistic simulations were performed using the M.Dynamix package[68] with standard periodic boundary conditions. Equations of motion were resolved by the Tuckerman−Berne double time step algorithm[69] with short and long time steps of 0.2 and 2.0 fs, respectively. The short time step is used for integrating fast intramolecular vibrations and nonbonded interactions within 5 Å, while the long time step is used for integrating VdW and

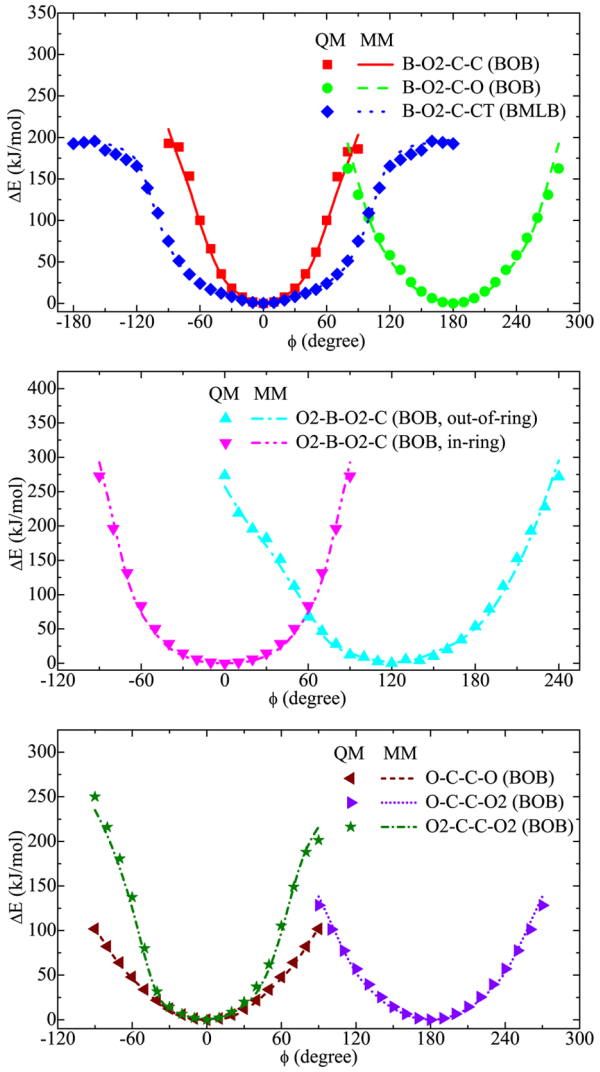

Figure 3. Typical torsion profiles of the dihedrals in [BMLB] and [BOB] anions, obtained from QM (dots) and MM (lines) calculations in this work. The notations of all atoms are shown in Figures S1 and S2 in the Supporting Information.

electrostatic forces within 15 Å, as well as dihedral angle motions. The electrostatic interactions between atom-centered point charges are treated with the standard Ewald summation method.

Atomistic simulations are carried out for all 12 halogen-free chelated orthoborate-phosphonium ILs in this study. Detailed simulation system compositions are listed in Table 7. All simulations are equilibrated for 5 ns in a Nosé−Hoover NPT ensemble at 333 K and under 1 atm with time coupling constants of 1000 and 30 fs, respectively. The equilibrated simulation box lengths for all simulation systems are listed in Table 7. The production phase persists another 10 ns, in which the trajectories are saved at an interval of 100 fs for further analysis. The last configuration of each simulation system is adopted to run atomistic simulations at 293, 313, 353, and 373 K, respectively, to take statistical data under different thermodynamic conditions.

Liquid Densities. The proposed FF can be validated by analyzing several properties, including liquid densities,[39,40,43,54,56] heat capacities,[40,54] spectroscopic data,[38,39,43] crystal structures,[40,41,55] self-diffusion coefficients,[38−40] etc.

Table 7. Simulation System Compositions of Halogen-Free Chelated Orthoborate-Phosphonium ILs and Equilibrated Box Sizes at 333 K[a]

ILs	no. of ion pairs	box length (Å)	ρ_{sim} (g/cm^3)	ρ_{exp} (g/cm^3)	error
[$P_{4,4,4,8}$][BMB]	128	50.47	1.0357 (0.0031)	1.0347	0.098%
[$P_{4,4,4,8}$][BMLB]	128	47.09	1.0817 (0.0033)		
[$P_{4,4,4,8}$][BOB]	128	46.22	1.0813 (0.0035)		
[$P_{4,4,4,8}$][BScB]	128	49.42	1.0548 (0.0033)	1.0521	0.254%
[$P_{4,4,4,14}$][BMB]	96	48.39	1.0003 (0.0034)	1.0148	−1.430%
[$P_{4,4,4,14}$][BMLB]	96	45.72	1.0275 (0.0035)		
[$P_{4,4,4,14}$][BOB]	96	44.91	1.0351 (0.0037)		
[$P_{4,4,4,14}$][BScB]	96	47.32	1.0277 (0.0035)	1.0144	1.310%
[$P_{6,6,6,14}$][BMB]	96	50.65	0.9749 (0.0029)	0.9845	−0.977%
[$P_{6,6,6,14}$][BMLB]	96	48.28	0.9894 (0.0031)	0.9479[b]	4.380%
[$P_{6,6,6,14}$][BOB]	96	47.13[c]	1.0215 (0.0028)[c]	0.99[d]	3.180%
			0.9478 (0.0033)[e]	0.9194[f]	3.089%
[$P_{6,6,6,14}$][BScB]	96	49.72	1.0001 (0.0029)	0.9942	0.598%

[a]The liquid densities calculated in this work (ρ_{sim}) at 333 K are compared with available experimental data (ρ_{exp}).[26] [b]Experimental liquid density for the synthesized [$P_{6,6,6,14}$][BMLB] IL sample with a water content of (0.391 ± 0.051) wt %.[26] [c]Equilibrated box size and simulated liquid density for neat [$P_{6,6,6,14}$][BOB] IL at 293 K. [d]Experimental liquid density for the [$P_{6,6,6,14}$][BOB] IL sample at 298 K.[70] [e]Simulated liquid density for the system containing 96 [$P_{6,6,6,14}$][BOB] ion pairs and 88 SPC/E water molecules, which leads to [$P_{6,6,6,14}$][BOB] IL with a water content of 2.4 wt %. This simulation system is adopted to mimic the synthesized [$P_{6,6,6,14}$][BOB] IL sample with a water content of 2.3−2.5 wt %.[26] [f]Experimental liquid density for the synthesized [$P_{6,6,6,14}$][BOB] IL sample with a water content of 2.3−2.5 wt %.[26]

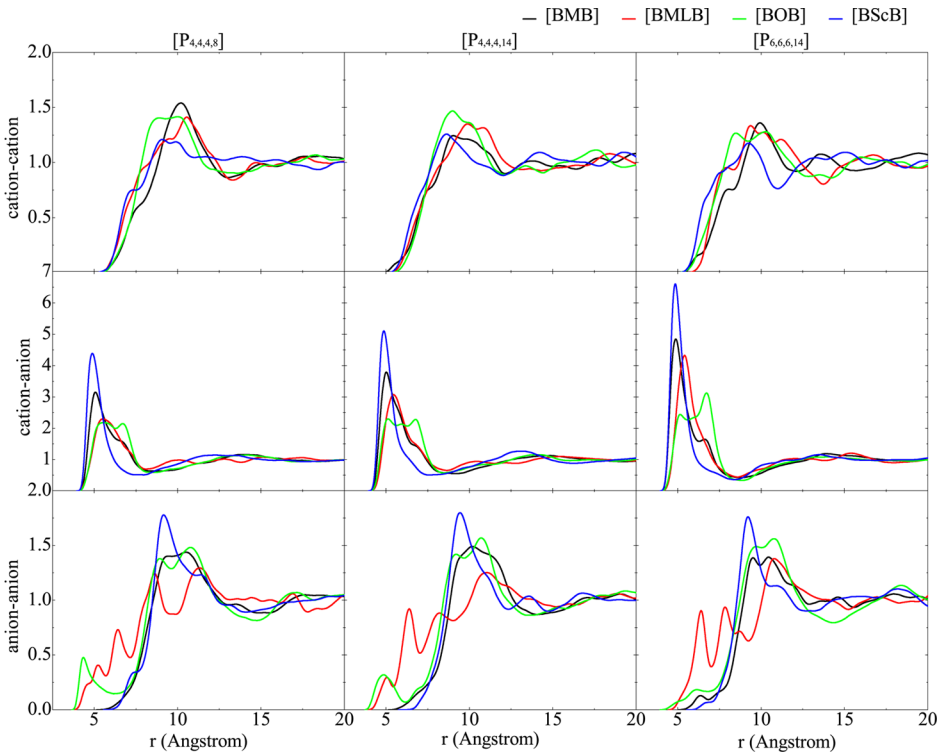

Figure 4. Site−site radial distribution functions between the P atom in tetraalkylphosphonium cations and the B atom in chelated orthoborate anions.

Liquid density is one of the most frequently used results to compare between experiments, as the value can be directly obtained from isothermal isobaric atomistic simulations.

As shown in Table 7 and Table S8 in the Supporting Information, within the investigated temperature range, all liquid densities of the 12 ILs exhibit linear variations, which is common behavior for halogen-free chelated orthoborate-phosphonium ILs[26] and other chelated orthoborate-based ILs.[71] The predicted densities in the temperature range 293−373 K agree well with available experimental data. Among all the density validations, most of the relative errors are within 2%, although some of them exceed 4%.

For the [$P_{6,6,6,14}$][BOB] IL, the liquid density calculated using the proposed FF is (1.0215 ± 0.0028) g/cm^3 at 293 K, which is consistent with the experimental value of 0.99 g/cm^3 from a water-free sample at 298 K.[70] However, the [$P_{6,6,6,14}$][BOB] IL is much more hygroscopic than the other halogen-free chelated orthoborate-phosphonium ILs and a small amount of water in the experiment can affect the corresponding liquid density. In the synthesized

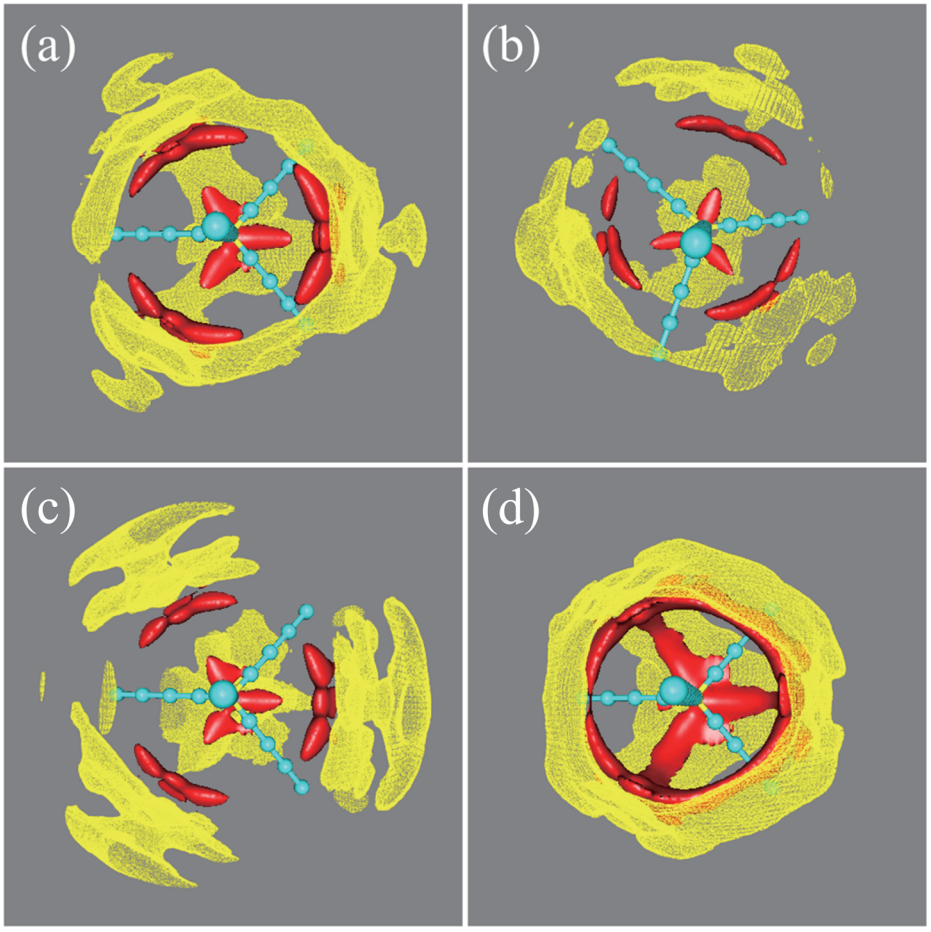

Figure 5. Three-dimensional probability distributions of the B atom (yellow meshed surface) and all oxygen atoms (red solid surface) in (a) [BMB], (b) [BMLB], (c) [BOB], and (d) [BScB] anions around the $[P_{4,4,4,8}]$ cation (P and carbon atoms are represented by yellow and cyan beads, respectively) obtained from atomistic simulations in this work. In each case, the red and yellow bounded contour surfaces are drawn at 5.5 and 4.0 times of average density, respectively.

$[P_{6,6,6,14}][BOB]$ IL sample,[26] the water content is 2.3−2.5 wt %. This amount of water is difficult to remove even after several iterative purifications including vacuum drying for a few hours at 85−90 °C. In our atomistic simulations, we added 88 SPC/E water molecules into the simulation box, leading to the $[P_{6,6,6,14}][BOB]$ IL with a water content of ∼2.4 wt %. The calculated liquid density is (0.9478 ± 0.0033) g/cm^3 at 333 K, which is close to the experimental value of 0.9194 g/cm^3 at the same temperature. Furthermore, we also found that using different water models, such as adopting the SPC, TIP3P, and TIP4P water models instead of the SPC/E model, has little effect on the liquid densities.

By comparing the effect of tetraalkylphosphonium cations, we found that the simulated densities decrease with an increase in the alkyl chain length in tetraalkylphosphonium cations where $[P_{4,4,4,8}]$ > $[P_{4,4,4,14}]$ > $[P_{6,6,6,14}]$ due to reduced interaction energies that lead to less efficient packing of ionic groups. While the effect of chelated orthoborate anions on predicted liquid densities is somewhat complicated, this may be attributed to the formation of intricate ionic structures of chelated orthoborate anions and elaborate interactions between ionic groups.

Components of Potential Energy. The breakdown of total potential energies into VdW, electrostatic, and bonded interaction energies is shown in Table S9 in the Supporting Information. The electrostatic interaction energies, which are several times larger than VdW interaction energies depending on anion size, contribute to the majority of the total potential energies and reflect the typical ionic feature of these liquids. It is interesting to note that all intramolecular parts of the VdW interaction energies are positive. By further analysis, we found that the intramolecular energies for tetraalkylphosphonium cations are positive, and increase with longer alkyl chain length. In optimized molecular geometries, as shown in the Supporting Information, all alkyl chains adopt *trans* conformations, which is one of the most stable structures and does not contribute to positive VdW energies. The positive intramolecular VdW energies indicate that the conformation of alkyl chains in the condensed liquid phase is quite different than that in the gas phase, which has been verified by X-ray crystallographic data of $[P_{10,10,10,10}][Br]$ and $[P_{18,18,18,18}][I]$ ILs.[60] For chelated orthoborate anions, the intramolecular VdW energies are positive, [BScB] > [BMLB] > [BMB] (from high to low, respectively), but negative for the [BOB] anion, as the value is related to the ionic size of these anions.

The intermolecular potential energy, heat of vaporization, molar volume, and cohesive energy density are also summarized in Table S9 in the Supporting Information. All of these halogen-free chelated orthoborate-phosphonium ILs exhibit extremely high values of heat of vaporization and cohesive energy density. Generally, smaller ionic group size leads to larger cohesive energy densities. Corresponding sequences for

the latter are $[P_{4,4,4,8}]$ > $[P_{4,4,4,14}]$ > $[P_{6,6,6,14}]$ for tetraalkylphosphonium cations and [BOB] > [BScB] > [BMLB] > [BMB] for chelated orthoborate anions.

Microscopic Structures. In Figure 4, we present the site−site radial distribution functions (RDFs) for cation−cation, cation−anion, and anion−anion pairs. The central P and B atoms are taken as reference sites of cations and anions to calculate corresponding site−site RDFs, which can depict the general microscopic ionic structures between ionic species. It is clearly demonstrated that local ionic structures of these ILs are strongly affected by the nature of tetraalkylphosphonium cations and chelated orthoborate anions.

For cation−cation and anion−anion RDFs, the long-range spatial correlations span beyond 20 Å. Such charge ordering phenomena are the intrinsic characteristics of a system dominated by long-range electrostatic interactions.[50] All of these cation−cation RDFs present very broad first maxima possessing more or less pronounced long-range shoulders. The RDFs between the anion−anion pair clearly present an anionic group size effect. For $[P_{4,4,4,8}]$-based ILs, the anion−anion RDFs in the last window of the first column in Figure 4 show short distance shoulders for [BOB] and [BMLB] anions due to their smaller anionic sizes. The shoulder positions are slightly shifted toward large distances with the increase of cationic group sizes.

According to the cation−anion RDFs, two distinct solvation shells are observed at around 5.0 and 14.0 Å, respectively, for [BMB]-, [BMLB]-, and [BScB]-based ILs. Broad distributions are observed in the first shell for [BOB]-based ILs. For the same anion, the cation−anion RDFs for such anion and tetraalkylphosphonium cations with larger alkyl groups exhibit a higher first peak and lower first minimum, indicating the formation of a well-defined first solvation shell of chelated orthoborate anions around tetraalkylphosphonium cations, and vice versa.

The organization of bulk liquid structures can also be analyzed by examining the coordination number, which is the average number of specific sites or atoms around the central atoms within a sphere of radius r. The coordination number, N, is calculated via the integral of RDFs from zero to the first minimum as $N = 4\pi\int_0^{R_{min1}} \rho g(r) r^2 \, dr$, where ρ is the number density and R_{min1} refers to the position of the first minimum in cation−anion RDFs. The calculated coordination numbers as well as the locations of the maximum and minimum in cation−anion RDFs of 12 ILs are listed in Table S10 in the Supporting Information.

From the coordination numbers for the P−B pair, it is evident that each ion is surrounded by several counterions. The tetraalkylphosphonium cations with longer alkyl chains have generally smaller coordination numbers due to steric effects of alkyl chains, which prevent chelated orthoborate anions from approaching the center of the tetraalkylphosphonium cations. Such ionic structures lead to less efficient packing of ionic groups around each other, and contribute to qualitative descriptions of liquid densities. For the same cation, the coordinate numbers increase with a decrease of anionic group sizes and follow the order of [BOB] > [BMLB] > [BMB] > [BScB].

The liquid structures are further depicted by spatial distribution functions (SDFs), which give the probability of finding an atom around a center molecule in three-dimensional space, in contrast to the average values given by RDFs. In this work, SDFs are visualized by the gOpenMol package.[72,73] As shown in Figure 5, the probability distributions of the B atom and all oxygen atoms in the chelated orthoborate anions around the $[P_{4,4,4,8}]$ cation are similar but have different characteristics. There are mainly four high probability domains for the B atom (yellow meshed surface), which contribute to the first solvation shell in corresponding RDFs (see the middle window of the first column in Figure 4 for reference). The largest densities are in the regions in the vicinity of the alkyl chains, which contributes to the strong static effect of the alkyl chains.

In the $[P_{4,4,4,8}]$[BOB] IL, each isolated domain is divided into two regions, which correspond to the double peaks in the first solvation shell in corresponding cation−anion RDFs. With one anion in each region, there are eight counterions in the first solvation shell. This observation agrees well with the calculated coordination number of 7.8 shown in Table S10 in the Supporting Information. With increased anionic group sizes, the differences between two regions in each domain become small, such that even adjacent domains are connected, as shown in Figure 5b, which contributes to a decrease in the coordination numbers. When two phenyl rings are attached to central segments, a pronounced difference between cations and anions is that each two adjacent domains are partially ([BMB] in Figure 5a) or totally ([BScB] in Figure 5d) connected to form network structures. Interestingly, we find that the SDFs of all oxygen atoms (red solid surface) in chelated orthoborate anions around the $[P_{4,4,4,8}]$ cation are characterized by three leaves, which are located within the domain between two alkyl chains. Such distributions are much like the structure of trefoil, as clearly shown in Figure 5.

Figure 6 shows the RDFs between the HP atoms in CH_2 groups connected to the central P atom in tetraalkylphospho-

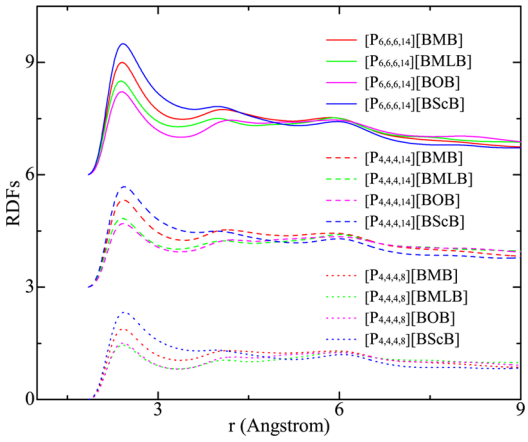

Figure 6. Site−site RDFs between the HP atoms in tetraalkylphosphonium cations and all oxygen atoms in chelated orthoborate anions. The RDFs for $[P_{4,4,4,14}]$- and $[P_{6,6,6,14}]$-based ILs are shifted 3 and 6 units, respectively, for easier comparison.

nium cations and all oxygen atoms in chelated orthoborate anions. The first peak height becomes more intense with increasing ionic group sizes, which are clearly clarified by SDFs of all oxygen atoms in the [BOB] anion around the HP atoms in tetraalkylphosphonium cations shown in Figure 7. In contrast to the P−B coordination numbers, tetraalkylphosphonium cations with longer alkyl chains or chelated orthoborate anions with larger ionic sizes have larger coordination numbers, as listed in Table S10 in the Supporting Information. Such abnormal phenomena are inconsistent with the traditional view that interactions between ionic groups become more difficult

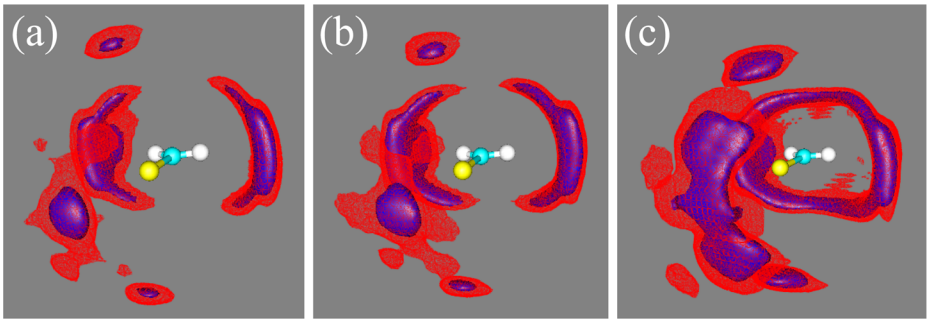

Figure 7. Three-dimensional probability distributions of all oxygen atoms in the [BOB] anion around HP atoms in (a) [$P_{4,4,4,8}$], (b) [$P_{4,4,4,14}$], and (c) [$P_{6,6,6,14}$] cations obtained from atomistic simulations in this work. In each case, we present the central P atom (yellow bead) and one adjacent CH_2 (carbon and hydrogen atoms are represented by cyan and white beads, respectively) group for clarity. The blue and red bounded contour surfaces are drawn at 5.5 and 4.0 times the average density, respectively.

for ILs with longer alkyl chains due to additional conformational flexibility and steric hindrance, which may contribute to the formation of hydrogen bonds between the HP atoms in tetraalkylphosphonium cations and all oxygen atoms in chelated orthoborate anions.[42]

Diffusion Coefficients. Figure 8 shows the log−log plot of typical mean square displacements (MSDs) of the [$P_{4,4,4,8}$] cation and the [BOB] anion at 333 K. All MSDs exhibit three dynamically different regimes, i.e., ballistic (MSD $\propto \Delta t^2$), subdiffusive (MSD $\propto \Delta t^{\beta}$ with $0 < \beta < 1$), and diffusive (MSD $\propto \Delta t$) regimes, in the whole diffusion process. The self-diffusion coefficients of ionic groups are obtained by a linear fitting of the slope of MSDs in the diffusive regime, and corresponding values are summarized in Table 8. The self-

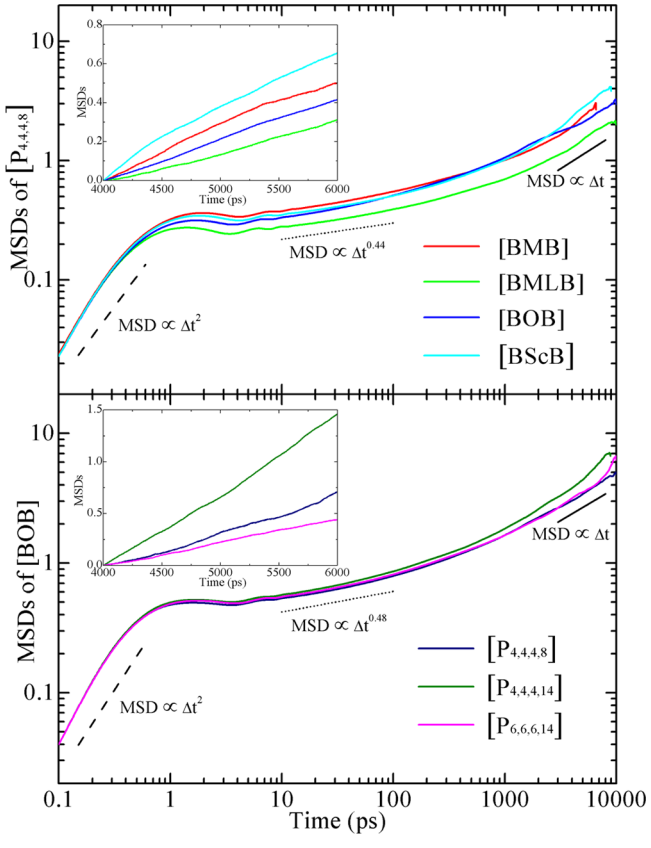

Figure 8. Log−log scale plot of MSDs (in Å^2) for diffusion of the [$P_{4,4,4,8}$] cation (top) in ILs with different chelated orthoborate anions and the [BOB] anion (bottom) in ILs with different tetraalkylphosphonium cations, respectively, at 333 K. The black dashed, dotted, and solid lines indicate diffusion of ionic groups in ballistic, subdiffusive, and diffusive regimes, respectively. The typical MSDs in the diffusive regime presented in the insets are adopted to fit self-diffusion coefficients of the [$P_{4,4,4,8}$] cation and the [BOB] anion, respectively.

Table 8. Self-Diffusion Coefficients (10^{-13} m^2/s) of Tetraalkylphosphonium Cations and Chelated Orthoborate Anions in 12 ILs Calculated from Atomistic Simulations at 333 K

	[$P_{4,4,4,8}$]		[$P_{4,4,4,14}$]		[$P_{6,6,6,14}$]	
	cation	anion	cation	anion	cation	anion
[BMB]	2.634	3.237	2.066	2.711	2.737	3.215
[BMLB]	1.648	1.825	1.780	2.588	2.645	2.818
[BOB]	2.079	3.630	5.521	7.357	2.054	2.254
[BScB]	3.280	3.431	2.645	2.851	3.073	4.178

diffusion coefficients of ionic groups of halogen-free chelated orthoborate-phosphonium ILs are on the order of 10^{-13} m^2/s, which is 3 orders of magnitude smaller than that of small molecules, such as water at room temperature.[74] Such slow diffusion of cations and anions is very common for other ILs.[39,46,50] The self-diffusion coefficients of the [$P_{6,6,6,14}$] cation and the [BMB] anion calculated in our atomistic simulations are 3 times smaller than the corresponding diffusion coefficients obtained from NMR experiments.[75]

As even the corresponding experimental data are limited,[75] Table 8 can give us some other physical insights. For [$P_{4,4,4,8}$]- and [$P_{4,4,4,14}$]-based ILs, experimental viscosity data reveal that the viscosity of [BMB] is greater than that of [BScB],[26] which results in corresponding diffusion with the order of [BMB] < [BScB], consistent with the calculated self-diffusion coefficients shown in Table 8. For [$P_{6,6,6,14}$]-based ILs, viscosities fall in the order of [BOB] > [BMB] > [BScB] > [BMLB],[26] and our calculated self-diffusion coefficients follow the order of [BOB] < [BMLB] < [BMB] < [BScB], which is generally consistent with experimental observations. These qualitative comparisons reveal that the proposed FF for halogen-free chelated orthoborate-phosphonium ILs provides reasonable insight into the dynamic feature of these ILs.

IV. CONCLUSIONS

In the present work, an all-atomistic FF for halogen-free chelated orthoborate-phosphonium ILs was developed on the

basis of the AMBER framework. Several types of parametrizations and systematic refinements were implemented in the development process. The VdW parameters lacking for the B atoms in chelated orthoborate anions are directly taken from the DREIDING FF. *Ab initio* quantum chemistry calculations were employed to obtain optimized molecular geometries, infrared frequencies, and torsion energy profiles. Atomic partial charges were obtained using standard one-conformation two-stage restraint electrostatic potential methodology to fit the molecular electrostatic potential generated from *ab initio* calculations. The bond and angle force constants were tuned to reproduce the vibration frequencies. Typical frequencies, including the P−C stretching frequency in tetraalkylphosphonium cations and the B−O2/OH stretching frequency in chelated orthoborate anions, were adjusted to fit corresponding experimental values. The missing torsion parameters of several dihedral angles in the AMBER FF were obtained by fitting corresponding torsion energy profiles from *ab initio* calculations.

The proposed FF was further validated by performing liquid phase atomistic simulations for 12 halogen-free chelated orthoborate-phosphonium ILs. The liquid densities predicted in this work are in good agreement with available experimental data. In addition, for the $[P_{6,6,6,14}][BOB]$ IL sample with a water content of 2.3−2.5 wt %, our proposed FF can correctly predict the experimentally measured liquid density. The analyses of potential energy components show that these ILs are dominated by strong electrostatic interactions between ionic species.

The RDFs and SDFs were employed to describe the microscopic ionic structures of these ionic liquids. The site−site RDFs between the P atom in tetraalkylphosphonium cations and the B atom in chelated orthoborate anions reveal obvious charge ordering phenomena in all of these ILs. The visualized images of SDFs clearly show three-dimensional probability distributions of atoms of interest around a central ionic group. There are mainly four high-probability regions of chelated orthoborate anions distributed around the tetraalkylphosphonium cations in the first solvation shell. The density distributions of the B atom and all oxygen atoms in chelated orthoborate anions around tetraalkylphosphonium cations are strongly influenced by anionic group sizes. The self-diffusion coefficients of tetraalkylphosphonium cations and chelated orthoborate anions, calculated from corresponding MSDs, indicate that the diffusion of these ionic groups is qualitatively consistent with available experimental viscosity data.

■ ASSOCIATED CONTENT

Supporting Information

Atom type notations and computed atomic partial charges of three tetraalkylphosphonium cations and four chelated orthoborate anions; typical optimized geometries of the $[P_{4,4,4,8}]$ cation and four chelated orthoborate anions obtained from QM *ab initio* calculations; detailed comparison of bond lengths and covalent bond angles in optimized ionic geometries of three tetraalkylphosphonium cations and four chelated orthoborate anions obtained from QM *ab initio* calculations with available experimental X-ray scattering data and other simulation results; comparison of quadrupole and octupole moments of symmetric ions obtained from QM *ab initio* calculations and RESP charges; detailed comparison of vibration frequencies of the $[P_{6,6,6,14}]$ cation, and [BMB] and [BScB] anions among QM calculations, MM fittings, and available experimental measurements; comparison of simulated liquid densities of 12 halogen-free chelated orthoborate-phosphonium ILs with available experimental data over a wide temperature range; comparison of various terms of potential energies, including VdW, electrostatic, and bonded interactions, heats of vaporization, molar volumes, and cohesive energy densities obtained from the atomistic simulations; structure of the $[P_{4,4,4,8}][BOB]$ ion pair with minimum energy optimized by QM *ab initio* calculations at the B3LYP/6-311++G(d) level; maximum and minimum positions for site−site RDFs and the first shell coordination numbers of 12 halogen-free chelated orthoborate-phosphonium ILs; details of Raman and ATR-FTIR experiments. This material is available free of charge via the Internet at http://pubs.acs.org.

■ AUTHOR INFORMATION

Corresponding Authors

*E-mail: yonglei.wang@mmk.su.se. Phone: 0046 8 162372. Fax: 0046 8 152187.

*E-mail: aatto.laaksonen@mmk.su.se. Phone: 0046 8 162372. Fax: 0046 8 152187.

Notes

The authors declare no competing financial interest.

■ ACKNOWLEDGMENTS

We gratefully acknowledge financial support from the Knut and Alice Wallenberg Foundation (Project number KAW 2012.0078) and the Swedish Research Council (Project number 2013-5171). The simulations were performed using resources provided by the Swedish National Infrastructure for Computing (SNIC) at PDC, HPC2N, and NSC. We thank Assoc. Prof. Allan Holmgren (LTU) for the assistance with ATR-FTIR and Raman experiments.

■ REFERENCES

(1) Greaves, T.; Drummond, C. Protic Ionic Liquids: Properties and Applications. *Chem. Rev.* **2008**, *108*, 206−237.

(2) Weingärtner, H. Understanding Ionic Liquids at the Molecular Level: Facts, Problems, and Controversies. *Angew. Chem., Int. Ed.* **2008**, *47*, 654−670.

(3) Fumino, K.; Fossog, V.; Wittler, K.; Hempelmann, R.; Ludwig, R. Dissecting Anion−Cation Interaction Energies in Protic Ionic Liquids. *Angew. Chem., Int. Ed.* **2013**, *52*, 2368−2372.

(4) Wasserscheid, P.; Keim, W. Ionic Liquids-New Solutions for Transition Metal Catalysis. *Angew. Chem., Int. Ed.* **2000**, *39*, 3772−3789.

(5) Rosen, B. A.; Salehi-Khojin, A.; Thorson, M. R.; Zhu, W.; Whipple, D. T.; Kenis, P. J.; Masel, R. I. Ionic Liquid−Mediated Selective Conversion of CO_2 to CO at Low Overpotentials. *Science* **2011**, *334*, 643−644.

(6) Allen, C.; Sambasivarao, S. V.; Acevedo, O. An Ionic Liquid Dependent Mechanism for Base Catalyzed β-Elimination Reactions from QM/MM Simulations. *J. Am. Chem. Soc.* **2013**, *135*, 1065−1072.

(7) Zhou, F.; Liang, Y.; Liu, W. Ionic Liquid Lubricants: Designed Chemistry for Engineering Applications. *Chem. Soc. Rev.* **2009**, *38*, 2590−2599.

(8) Han, X.; Armstrong, D. Ionic Liquids in Separations. *Acc. Chem. Res.* **2007**, *40*, 1079−1086.

(9) Armand, M.; Endres, F.; MacFarlane, D.; Ohno, H.; Scrosati, B. Ionic-Liquid Materials for the Electrochemical Challenges of the Future. *Nat. Mater.* **2009**, *8*, 621−629.

(10) Liu, H.; Liu, Y.; Li, J. Ionic Liquids in Surface Electrochemistry. *Phys. Chem. Chem. Phys.* **2010**, *12*, 1685−1697.

(11) Gebbie, M. A.; Valtiner, M.; Banquy, X.; Fox, E. T.; Henderson, W. A.; Israelachvili, J. N. Ionic Liquids Behave as Dilute Electrolyte Solutions. *Proc. Natl. Acad. Sci. U.S.A.* **2013**, *110*, 9674−9679.
(12) Del Sesto, R. E.; Corley, C.; Robertson, A.; Wilkes, J. S. Tetraalkylphosphonium-Based Ionic Liquids. *J. Organomet. Chem.* **2005**, *690*, 2536−2542.
(13) Cieniecka-Rosłonkiewicz, A.; Pernak, J.; Kubis-Feder, J.; Ramani, A.; Robertson, A. J.; Seddon, K. R. Synthesis, Anti-Microbial Activities and Anti-Electrostatic Properties of Phosphonium-Based Ionic Liquids. *Green Chem.* **2005**, *7*, 855−862.
(14) Kagimoto, J.; Fukumoto, K.; Ohno, H. Effect of Tetrabutylphosphonium Cation on the Physico-Chemical Properties of Amino-Acid Ionic Liquids. *Chem. Commun.* **2006**, 2254−2256.
(15) Kagimoto, J.; Nakamura, N.; Kato, T.; Ohno, H. Novel Thermotropic Gels Composed of Only Ions. *Chem. Commun.* **2009**, 2405−2407.
(16) Armel, V.; Rivnay, J.; Malliaras, G.; Winther-Jensen, B. Unexpected Interaction Between PEDOT and Phosphonium Ionic Liquids. *J. Am. Chem. Soc.* **2013**, *135*, 11309−11313.
(17) Zhang, J.; Zhang, S.; Dong, K.; Zhang, Y.; Shen, Y.; Lv, X. Supported Absorption of CO_2 by Tetrabutylphosphonium Amino Acid Ionic Liquids. *Chem.—Eur. J.* **2006**, *12*, 4021−4026.
(18) Gardas, R. L.; Ge, R.; Goodrich, P.; Hardacre, C.; Hussain, A.; Rooney, D. W. Thermophysical Properties of Amino Acid-Based Ionic Liquids. *J. Chem. Eng. Data* **2009**, *55*, 1505−1515.
(19) Goodrich, B. F.; de la Fuente, J. C.; Gurkan, B. E.; Zadigian, D. J.; Price, E. A.; Huang, Y.; Brennecke, J. F. Experimental Measurements of Amine-Functionalized Anion-Tethered Ionic Liquids with Carbon Dioxide. *Ind. Eng. Chem. Res.* **2010**, *50*, 111−118.
(20) Goodrich, B. F.; de la Fuente, J. C.; Gurkan, B. E.; Lopez, Z. K.; Price, E. A.; Huang, Y.; Brennecke, J. F. Effect of Water and Temperature on Absorption of CO_2 by Amine-Functionalized Anion-Tethered Ionic Liquids. *J. Phys. Chem. B* **2011**, *115*, 9140−9150.
(21) Niedermaier, I.; Bahlmann, M.; Papp, C.; Kolbeck, C.; Wei, W.; Krick Calderon, S.; Grabau, M.; Schulz, P. S.; Wasserscheid, P.; Steinrück, H.-P.; et al. Carbon Dioxide Capture by An Amine Functionalized Ionic Liquid: Fundamental Differences of Surface and Bulk Behavior. *J. Am. Chem. Soc.* **2014**, *136*, 436−441.
(22) Tsunashima, K.; Sugiya, M. Physical and Electrochemical Properties of Low-Viscosity Phosphonium Ionic Liquids as Potential Electrolytes. *Electrochem. Commun.* **2007**, *9*, 2353−2358.
(23) Fraser, K. J.; MacFarlane, D. R. Phosphonium-Based Ionic Liquids: An Overview. *Aust. J. Chem.* **2009**, *62*, 309−321.
(24) Yu, S.; Lindeman, S.; Tran, C. D. Chiral Ionic Liquids: Synthesis, Properties, and Enantiomeric Recognition. *J. Org. Chem.* **2008**, *73*, 2576−2591.
(25) Chiappe, C.; Signori, F.; Valentini, G.; Marchetti, L.; Pomelli, C. S.; Bellina, F. Novel (Glycerol)borate-Based Ionic Liquids: An Experimental and Theoretical Study. *J. Phys. Chem. B* **2010**, *114*, 5082−5088.
(26) Shah, F. U.; Glavatskih, S.; MacFarlane, D. R.; Somers, A.; Forsyth, M.; Antzutkin, O. N. Novel Halogen-Free Chelated Orthoborate−Phosphonium Ionic Liquids: Synthesis and Tribophysical Properties. *Phys. Chem. Chem. Phys.* **2011**, *13*, 12865−12873.
(27) Shah, F. U.; Glavatskih, S.; Dean, P. M.; MacFarlane, D. R.; Forsyth, M.; Antzutkin, O. N. Halogen-Free Chelated Orthoborate Ionic Liquids and Organic Ionic Plastic Crystals. *J. Mater. Chem.* **2012**, *22*, 6928−6938.
(28) Wang, Y.; Jiang, W.; Yan, T.; Voth, G. A. Understanding Ionic Liquids Through Atomistic and Coarse-Grained Molecular Dynamics Simulations. *Acc. Chem. Res.* **2007**, *40*, 1193−1199.
(29) Bhargava, B.; Balasubramanian, S.; Klein, M. L. Modelling Room Temperature Ionic Liquids. *Chem. Commun.* **2008**, 3339−3351.
(30) Gutowski, K. E.; Maginn, E. J. Amine-Functionalized Task-Specific Ionic Liquids: A Mechanistic Explanation for the Dramatic Increase in Viscosity Upon Complexation with CO_2 From Molecular Simulation. *J. Am. Chem. Soc.* **2008**, *130*, 14690−14704.
(31) Zhao, W.; Leroy, F.; Heggen, B.; Zahn, S.; Kirchner, B.; Balasubramanian, S.; Müller-Plathe, F. Are There Stable Ion-Pairs in Room-Temperature Ionic Liquids? Molecular Dynamics Simulations of 1-n-Butyl-3-Methylimidazolium Hexafluorophosphate. *J. Am. Chem. Soc.* **2009**, *131*, 15825−15833.
(32) Wendler, K.; Dommert, F.; Zhao, Y. Y.; Berger, R.; Holm, C.; Delle Site, L. Ionic Liquids Studied Across Different Scales: A Computational Perspective. *Faraday Discuss.* **2012**, *154*, 111−132.
(33) Beichel, W.; Trapp, N.; Hauf, C.; Kohler, O.; Eickerling, G.; Scherer, W.; Krossing, I. Charge-Scaling Effect in Ionic Liquids From the Charge-Density Analysis of N,N-Dimethylimidazolium Methylsulfate. *Angew. Chem., Int. Ed.* **2014**, *53*, 3143−3146.
(34) Yan, F.; Xia, S.; Wang, Q.; Yang, Z.; Ma, P. Predicting the Melting Points of Ionic Liquids by the Quantitative Structure Property Relationship Method Using a Topological Index. *J. Chem. Thermodyn.* **2013**, *62*, 196−200.
(35) Butler, S. N.; Müller-Plathe, F. A Molecular Dynamics Study of Viscosity in Ionic Liquids Directed by Quantitative Structure−Property Relationships. *ChemPhysChem* **2012**, *13*, 1791−1801.
(36) Couling, D. J.; Bernot, R. J.; Docherty, K. M.; Dixon, J. K.; Maginn, E. J. Assessing the Factors Responsible for Ionic Liquid Toxicity to Aquatic Organisms via Quantitative Structure−Property Relationship Modeling. *Green Chem.* **2006**, *8*, 82−90.
(37) De Andrade, J.; Böes, E. S.; Stassen, H. Computational Study of Room Temperature Molten Salts Composed by 1-Alkyl-3-Methylimidazolium Cations Force-Field Proposal and Validation. *J. Phys. Chem. B* **2002**, *106*, 13344−13351.
(38) Morrow, T. I.; Maginn, E. J. Molecular Dynamics Study of the Ionic Liquid 1-n-Butyl-3-Methylimidazolium Hexafluorophosphate. *J. Phys. Chem. B* **2002**, *106*, 12807−12813.
(39) Liu, Z.; Huang, S.; Wang, W. A Refined Force Field for Molecular Simulation of Imidazolium-Based Ionic Liquids. *J. Phys. Chem. B* **2004**, *108*, 12978−12989.
(40) Cadena, C.; Maginn, E. J. Molecular Simulation Study of Some Thermophysical and Transport Properties of Triazolium-Based Ionic Liquids. *J. Phys. Chem. B* **2006**, *110*, 18026−18039.
(41) Lopes, J. N. C.; Padua, A. A. H. Molecular Force Field for Ionic Liquids III: Imidazolium, Pyridinium, and Phosphonium Cations; Chloride, Bromide, and Dicyanamide Anions. *J. Phys. Chem. B* **2006**, *110*, 19586−19592.
(42) Liu, X.; Zhao, Y.; Zhang, X.; Zhou, G.; Zhang, S. Microstructures and Interaction Analyses of Phosphonium-Based Ionic Liquids: A Simulation Study. *J. Phys. Chem. B* **2012**, *116*, 4934−4942.
(43) De Andrade, J.; Böes, E. S.; Stassen, H. A Force Field for Liquid State Simulations on Room Temperature Molten Salts: 1-Ethyl-3-Methylimidazolium Tetrachloroaluminate. *J. Phys. Chem. B* **2002**, *106*, 3546−3548.
(44) Del Pópolo, M. G.; Voth, G. A. On the Structure and Dynamics of Ionic Liquids. *J. Phys. Chem. B* **2004**, *108*, 1744−1752.
(45) Micaelo, N. M.; Baptista, A. M.; Soares, C. M. Parametrization of 1-Butyl-3-Methylimidazolium Hexafluorophosphate/Nitrate Ionic Liquid for the GROMOS Force Field. *J. Phys. Chem. B* **2006**, *110*, 14444−14451.
(46) Bhargava, B.; Balasubramanian, S. Refined Potential Model for Atomistic Simulations of Ionic Liquid [BMIM][PF_6]. *J. Chem. Phys.* **2007**, *127*, 114510.
(47) Jacquemin, J.; Husson, P.; Mayer, V.; Cibulka, I. High-Pressure Volumetric Properties of Imidazolium-Based Ionic Liquids: Effect of the Anion. *J. Chem. Eng. Data* **2007**, *52*, 2204−2211.
(48) Borodin, O. Polarizable Force Field Development and Molecular Dynamics Simulations of Ionic Liquids. *J. Phys. Chem. B* **2009**, *113*, 11463−11478.
(49) Sambasivarao, S. V.; Acevedo, O. Development of OPLS-AA Force Field Parameters for 68 Unique Ionic Liquids. *J. Chem. Theory Comput.* **2009**, *5*, 1038−1050.
(50) Wang, Y.-L.; Lyubartsev, A.; Lu, Z.-Y.; Laaksonen, A. Multiscale Coarse-Grained Simulations of Ionic Liquids: Comparison of Three Approaches to Derive Effective Potentials. *Phys. Chem. Chem. Phys.* **2013**, *15*, 7701−7712.
(51) Wang, Y.-L.; Laaksonen, A.; Lu, Z.-Y. Influence of Ionic Liquid Film Thickness on Ion Pair Distributions and Orientations at

Graphene and Vacuum Interfaces. *Phys. Chem. Chem. Phys.* **2013**, *15*, 13559−13569.
(52) Paschek, D.; Köddermann, T.; Ludwig, R. Solvophobic Solvation and Interaction of Small Apolar Particles in Imidazolium-Based Ionic Liquids. *Phys. Rev. Lett.* **2008**, *100*, 115901.
(53) Chaumont, A.; Wipff, G. Solvation of M^{3+} Lanthanide Cations in Room-Temperature Ionic Liquids. A Molecular Dynamics Investigation. *Phys. Chem. Chem. Phys.* **2003**, *5*, 3481−3488.
(54) Zhou, G.; Liu, X.; Zhang, S.; Yu, G.; He, H. A Force Field for Molecular Simulation of Tetrabutylphosphonium Amino Acid Ionic Liquids. *J. Phys. Chem. B* **2007**, *111*, 7078−7084.
(55) Canongia Lopes, J. N.; Deschamps, J.; Pádua, A. A. Modeling Ionic Liquids Using A Systematic All-Atom Force Field. *J. Phys. Chem. B* **2004**, *108*, 2038−2047.
(56) Canongia Lopes, J. N.; Pádua, A. A. Molecular Force Field for Ionic Liquids Composed of Triflate or Bistriflylimide Anions. *J. Phys. Chem. B* **2004**, *108*, 16893−16898.
(57) Cornell, W. D.; Cieplak, P.; Bayly, C. I.; Gould, I. R.; Merz, K. M.; Ferguson, D. M.; Spellmeyer, D. C.; Fox, T.; Caldwell, J. W.; Kollman, P. A. A Second Generation Force Field for the Simulation of Proteins, Nucleic Acids, and Organic Molecules. *J. Am. Chem. Soc.* **1995**, *117*, 5179−5197.
(58) Mayo, S. L.; Olafson, B. D.; Goddard, W. A., III. DREIDING: A Generic Force Field for Molecular Simulations. *J. Phys. Chem.* **1990**, *94*, 8897−8909.
(59) Frisch, M. J.; Trucks, G. W.; Schlegel, H. B.; Scuseria, G. E.; Robb, M. A.; Cheeseman, J. R.; Scalmani, G.; Barone, V.; Mennucci, B.; Petersson, G. A.; et al. *Gaussian 09*, revision A.02; Gaussian, Inc.: Wallingford, CT, 2009.
(60) Abdallah, D. J.; Bachman, R. E.; Perlstein, J.; Weiss, R. G. Crystal Structures of Symmetrical Tetra-n-Alkyl Ammonium and Phosphonium Halides. Dissection of Competing Interactions Leading to Biradial and Tetraradial Shapes. *J. Phys. Chem. B* **1999**, *103*, 9269−9278.
(61) Yang, M.; Xu, F.; Liu, Q.; Yan, P.; Liu, X.; Wang, C.; Welz-Biermann, U. Chelated Orthoborate Ionic Liquid as A Reactant for the Synthesis of A New Cobalt Borophosphate Containing Extra-Large 16-Ring Channels. *Dalton Trans.* **2010**, *39*, 10571−10573.
(62) Yang, M.; Yan, P.; Xu, F.; Ma, J.; Welz-Biermann, U. Role of Boron-Containing Ionic Liquid in the Synthesis of Manganese Borophosphate With Extra-large 16-Ring Pore Openings. *Microporous Mesoporous Mater.* **2012**, *147*, 73−78.
(63) Bayly, C. I.; Cieplak, P.; Cornell, W.; Kollman, P. A. A Well-Behaved Electrostatic Potential Based Method Using Charge Restraints for Deriving Atomic Charges: The RESP Model. *J. Phys. Chem.* **1993**, *97*, 10269−10280.
(64) Wang, J.; Cieplak, P.; Kollman, P. A. How Well Does A Restrained Electrostatic Potential (RESP) Model Perform in Calculating Conformational Energies of Organic and Biological Molecules? *J. Comput. Chem.* **2000**, *21*, 1049−1074.
(65) Scott, A. P.; Radom, L. Harmonic Vibrational Frequencies: An Evaluation of Hartree-Fock, Møller-Plesset, Quadratic Configuration Interaction, Density Functional Theory, and Semiempirical Scale Factors. *J. Phys. Chem.* **1996**, *100*, 16502−16513.
(66) Pappu, R. V.; Hart, R. K.; Ponder, J. W. Analysis and Application of Potential Energy Smoothing and Search Methods for Global Optimization. *J. Phys. Chem. B* **1998**, *102*, 9725−9742.
(67) Murphy, L. J.; McPherson, A. M.; Robertson, K. N.; Clyburne, J. A. Ionic Liquids and Acid Gas Capture: Water and Oxygen as Confounding Factors. *Chem. Commun.* **2012**, *48*, 1227−1229.
(68) Lyubartsev, A.; Laaksonen, A. M. DynaMix-A Scalable Portable Parallel MD Simulation Package for Arbitrary Molecular Mixtures. *Comput. Phys. Commun.* **2000**, *128*, 565−589.
(69) Tuckerman, M.; Berne, B.; Martyna, G. Reversible Multiple Time Scale Molecular Dynamics. *J. Chem. Phys.* **1992**, *97*, 1990−2001.
(70) Lall-Ramnarine, S. I.; Castano, A.; Subramaniam, G.; Thomas, M. F.; Wishart, J. F. Synthesis, Characterization and Radiolytic Properties of Bis(oxalato)borate Containing Ionic Liquids. *Radiat. Phys. Chem.* **2009**, *78*, 1120−1125.
(71) Xu, W.; Wang, L.-M.; Nieman, R. A.; Angell, C. A. Ionic Liquids of Chelated Orthoborates as Model Ionic Glassformers. *J. Phys. Chem. B* **2003**, *107*, 11749−11756.
(72) Laaksonen, L. A Graphics Program for the Analysis and Display of Molecular Dynamics Trajectories. *J. Mol. Graphics* **1992**, *10*, 33−34.
(73) Bergman, D. L.; Laaksonen, L.; Laaksonen, A. Visualization of Solvation Structures in Liquid Mixtures. *J. Mol. Graphics Modell.* **1997**, *15*, 301−306.
(74) van Dam, L.; Lyubartsev, A. P.; Laaksonen, A.; Nordenskiöld, L. Self-Diffusion and Association of Li^+, Cs^+, and H_2O in Oriented DNA Fibers. An NMR and MD Simulation Study. *J. Phys. Chem. B* **1998**, *102*, 10636−10642.
(75) Filippov, A.; Shah, F.; Taher, M.; Glavatskih, S.; Antzutkin, O. N. NMR Self-Diffusion Study of a Phosphonium Bis(mandelato)-borate Ionic Liquid. *Phys. Chem. Chem. Phys.* **2013**, *15*, 9281−9287.